Towards Mail-in-Sensors for SARS-CoV-2 Detection: Interfacing Gel Switch Resonators with Cell-free Toehold Switches

Authors: Adam R. Carr[1,†], Jared L. Dopp[1,†],Kaiyue Wu[2], Peivand Sadat Mousavi[3], Yeong Ran Jo[1], Ciara E. McNeley[1], Zachary T. Lynch[1], Keith Pardee[3], Alexander A. Green[2], Nigel F. Reuel[1,*]

1. Department of Chemical and Biological Engineering, Iowa State University, Ames, Iowa 50011, United States
2. Department of Biomedical Engineering, Boston University, Boston, Massachusetts 02215, United States
3. University of Toronto, Leslie Dan Faculty of Pharmacy, Toronto, ON M5S 1A1, Canada

[†] Authors contributed equally
[*] Corresponding author – reuel@iastate.edu

Keywords SARS-CoV-2, biosensor, toehold switch, LC resonator, viral diagnostic

Abstract

The COVID-19 pandemic has emphasized the importance of widespread testing to control spread of infectious disease. The rapid development, scale-up, and deployment of viral and antibody detection methods since the beginning of the pandemic have greatly increased testing capacity. Desirable attributes of detection methods are low product costs, self-administered protocols, and the ability to be mailed in sealed envelopes for safe analysis and subsequent logging to public health databases. Herein such a platform is demonstrated with a screen-printed, inductor-capacitor (LC) resonator as transducer and a toehold switch coupled with cell free expression as the biological selective recognition element. In the presence of the N-gene from SARS-CoV-2, the toehold switch relaxes, protease enzyme is expressed and it degrades a gelatin switch that ultimately shifts the resonant frequency of the planar resonant sensor. The gelatin switch resonator (GSR) can be analyzed through a sealed envelope allowing for assessment without the need of careful sample handling with personal protective equipment or need of workup with other reagents. The toehold switch used in this sensor demonstrated selectivity to SARS-CoV-2 virus over three seasonal coronaviruses and SARS-CoV-1 with a limit of detection of 100 copies/µL. Functionality of the platform and assessment in a sealed envelope with an automated scanner is shown with overnight shipment, and further improvements are discussed to increase signal stability and further simplify user protocols towards a mail-in platform.

The COVID-19 pandemic, caused by severe acute respiratory syndrome coronavirus 2 (SARS-CoV-2), has disrupted global supply chains, exposed the fragility of worldwide health systems, and caused millions of deaths.[1] This is partially due to the highly infectious nature of SARS-CoV-2, which led to uncontrolled spread across the globe. Person-to-person transmission of the virus can occur even in infected individuals with mild symptoms or no symptoms at all.[2,3] The

gold standard for SARS-CoV-2 detection is real-time reverse transcription polymerase chain reaction (rRT-PCR) assays that are conducted in centralized labs.[4,5] A benefit of centralized testing is the ability to build public health databases to reliably track patterns in outbreaks. However, this centralized method has limitations such as longer time to result, the high cost of rRT-PCR instruments , and the large PPE footprint for both sample collection and processing of the sample at a laboratory facility.[6–10] Sensing platforms are needed that allow for at home testing to eliminate the need of PPE yet allow for centralized readings to collect public health data. Such an approach would also improve access to testing.

Despite the success in efficacy (>90%) of mRNA vaccine delivery technology, many in the world remain at risk of infection, especially in low- and middle- income nations with limited access to testing facilities and vaccination clinics. At the same time, the ongoing pandemic has led to the emergence of new, more infectious variants, such as the Omicron variant, that could lead to increases in hospitalizations and reductions in vaccine effectiveness.[11–16] The emergence of these variants is a sign that SARS-CoV-2 is an ongoing public health crisis and further necessitates the development of reliable, rapid tests that can provide a diagnosis at the point-of-need (PON). Multiple tests have been developed using isothermal amplification techniques and CRISPR proteins that result in a colorimetric or fluorometric signal.[17–19] While these methods may be sensitive and specific, they still require reading on a centralized machine (e.g., plate reader) that would necessitate sample handling (thereby returning PPE burden). Conceivably, such colorimetric techniques could be printed on paper and read through a transparent window of a mailer, but this would risk privacy issues. Also, if the colorimetric readout could be discerned by eye, users would have little incentive to send in their results and public health databases would not have timely access to results.

In this work, a sensor platform is developed and tested that would allow for 1) sampling of virus at home without PPE, 2) mailing in a sealed envelope and 3) reading at a centralized location through the sealed envelope without making product contact thereby allowing for aggregating demographic data of the outbreak. The sensor platform consists of a gene-circuit regulating cell-free expression coupled to passive resonators as a contactless transduction element. An external reader antenna connected to a low-cost, portable, vector network analyzer allows for contactless interrogation of the sensor through a sealed envelope. The sensor protocol begins with an off-sensor amplification step of sample viral RNA into DNA using reverse transcription recombinase polymerase amplification (RT-RPA). The amplified DNA is then added to a cell-free expression (CFE) reaction that harbors a toehold switch regulating expression of the hydrolytic reporter enzyme, a protease subtilisin BPN' (SBT(n)), in response to a sequence of interest, in this case a portion of the N-gene in the SARS-CoV-2 genome. The CFE reaction is run on top of a gelatin layer covering a resonant sensor device. When the gelatin is degraded, a shift in resonant frequency can be observed using the vector network analyzer (VNA), Fig. 1 sensor protocol diagram. Since the gel layer induces the resonator frequency change, we refer to the combined gel/resonator system as a gel switch resonator (GSR). We demonstrate that this sensor platform can be used to detect SARS-CoV-2 viral samples from Washington (WA) and Hong Kong (HK) strains while rejecting off-target coronaviruses (e.g., SARS-CoV-1).

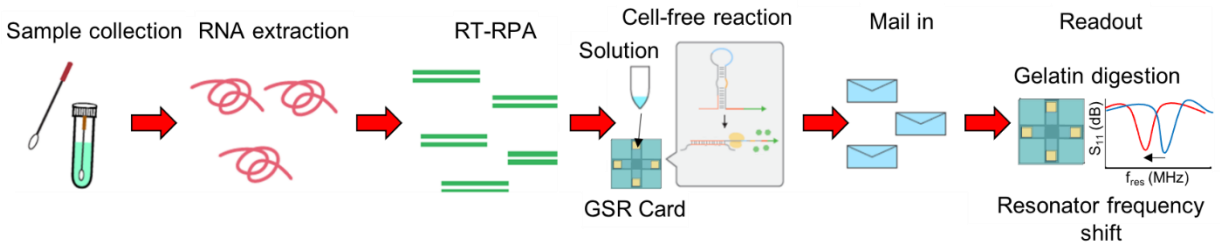

Figure 1. GSR test flow diagram starting with sample collection, extraction of viral RNA material, isothermal amplification via RT-RPA, cell-free reaction and sample application on GSR, mail-in test, and readout monitoring frequency shifts.

Materials and methods

GSR Design and Fabrication

Resonators were designed *in silico* to determine the effect of degradation of gelatin on resonant sensor. This was simulated using a finite element method (FEM) solver High Frequency Structure Simulator (HFSS) in the Ansys Electronic Desktop software package. The solution frequency was set to 100 MHz with a frequency sweep of 1 – 180 MHz with 6 passes.

To validate the results obtained from HFSS simulations printer paper dielectric properties were tested in both a dry and wet state. Dielectric properties of paper were tested using dielectric test meter (HP 16451B). Papers were either left dry or applied with 30 µL of PBS buffer in each port and allowed to sit at room temperature for moisture to absorb into the card. Papers were then sealed in envelopes and placed in between the plates of the dielectric test meter fitted to a four-port impedance analyzer (Agilent 4192A). Envelopes were used to determine if dielectric properties could be interrogated through the envelope. The reactance was recorded at 35.54 MHz to determine relative changes in capacitance between wet and dry paper

Materials for the GSR card include printer paper, polyethylene teraphthalate (PET, Melinex ST505, SWM International) double-stick tape (ATack clear, Amazon), gelatin (Great Value, Walmart), parafilm (Millipore Sigma), conductive ink (Dupont DP 5028), and solid wax ink (Professor Color). Resonant sensors were screen printed on paper using a previously reported protocol[20]. In brief, a paper was taped to a PET sheet and placed on a screen printer. Conductive ink loaded onto a screen with spiral resonant designs was pneumatically pressed through with a squeegee onto the paper. The paper was cured in an oven for 15 minutes at 120 °C. Wax printed channels were prepared with solid ink using a wax printer (Xerox ColorQube 8580) and adhered on top of the resonator with a laser cut piece of double-stick tape. The laser-cut pattern consisted of cross cuts to connect the four channels of the wax printed paper with the resonator. Gelatin 10 wt% was mixed with double deionized water and mixed at 90 °C until dissolved and cast in petri dish. Solidified gelatin was then cut and placed on the edge of the four channels on the GSR card. The gelatin was desiccated under a vacuum for one hour. Finally, parafilm with ports laser cut for the desiccated gelatin was adhered to the top of the GSR card to prevent samples from spilling over the GSR card.

GSR Test Protocol

Before being tested with a sample, GSR cards were scanned in envelopes in a custom-built scanner to get their baseline resonant frequency. The scanner consisted of a vector network analyzer (Copper Mountain TR1300), linear translation stage (THORLABS KMTS50E/M), and two-coil antenna/holder laser cut in acrylic with a 25x15 cm base for the translation stage and 15x10 cm head for the antenna. The vector network analyzer was setup to scan between 1 and 250 MHz using 5000 points. The linear stage translated the card 2.5 mm in 0.5 mm steps. These translation steps were used to minimize signal noise due to misalignment between the reader and card since the card would be removed and replaced in the reader to be tested with a sample. More information on the scanning method and validation experiments can be found in Supplement 1. The cards were tested with either samples of concentrated bacterial protease (Carolina Biologic, concentration unknown) or SBT(n) protease produced in cell-free reactions (see below section 2.5 for details on cell-free reactions). For bacterial protease samples, the enzyme cocktail was diluted with PBS buffer in a 1:10 mixture and cell-free reactions were always done at 10-µL reaction volumes diluted with 20 µL of PBS for a working volume of 30 µL on the card. The scanner saved the frequency sweep of the S_{11} scattering parameter at all six steps of the linear translation stage motion. A quadratic model was fit around the global minimum of each scan and the resonant frequency was set at the minimum of the model. All signal processing of scans for the GSR cards were carried out in Matlab using custom scripts, see Supplement 2. All tests sent through the mail received approval form the Export Compliance Program in the Office of Research Ethics at Iowa State University in accordance with United States federal laws regulating shipment of research materials internationally.

In Silico Toehold Switch Selection

Toehold switches targeting the antisense N gene of the SARS-CoV-2 viral RNA were designed using NUPACK-assisted design algorithms[21]. Full target and toehold switch sequence information can be found in Supplement 3. To increase the likelihood of getting an optimal design, two design parameters described in previous publications[22–24] were used to generate a library of designs. Multiple RNA defect levels were computed to provide measures of the deviation of each sensor from the ideal toehold switch secondary structure. A scoring function based on these defect levels was implemented to rank all designs in the library. Eleven top toehold switch designs for the SARS-CoV-2 target sites were selected for subsequent empirical testing. Linear DNA constructs harboring the toehold sequences were initially screened using I*n Vitro* Protein PURExpress kit (New England Biolabs) using *LacZ* as a reporter gene, which catalyzes cleavage of a yellow substrate termed Chlorophenol red-β-D-galactopyranoside and produces a purple product. After down selection of toehold switches based on *LacZ* as the reporter gene, the toehold switches were made with the gene expressing SBT(n) and assayed according to protocols described in section 2.5 below.

In Silico RPA Primer Design and Isothermal Amplification of RNA

RPA primers were designed *in silico* at sites located within ±40 nucleotides (nts) of the binding site of the toehold switch based on RPA manufacturer recommendations. Candidate primers are 30-38 nts in length with 40-60% in GC content. They were also checked for internal secondary structures and the probability of primer dimer formation. The T7 promoter sequence: GCGCTAATACGACTCACTATAGGG is added to the forward RPA primers to allow for transcription of the amplicons.

The TwistAmp Liquid Basic kit (TwistDx, United Kingdom) was used for all RPA reactions. The reactions were carried out according to manufacturer's protocol. Synthetic DNA oligos (IDT) were used as templates to generate synthetic viral RNA in initial experiments. For RT-RPA, 2.5 µL of M-MuLV reverse transcriptase (NEB) was added to the RPA reaction in addition to 2 µL of viral RNA sample. Reactions were run for 1 h at 42 °C. The resulting DNA was purified using a DNA clean and concentrator kit (Zymo Research, D4013) and eluted in ddH_2O. DNA trigger template concentration was quantified using a spectrophotometer (Implen NP80) and the templates were stored at -20 °C or used directly for *in vitro* transcription. *In vitro* transcription was carried out using an AmpliScribe T7-Flash transcription kit (Lucigen). Reactions were assembled according to the manufacturer protocols with 5 µL DNA. Reactions were run for 2 h at 42°C. Completed reactions were treated with DNase per the manufacture protocol. RNA trigger concentration was quantified using a spectrophotometer (Implen NP80) and triggers were stored at -80 °C or used directly in CFE.

Cell-free Reactions and SBT(N) Activity Assay

CFE reactions using the PANOx-SP energy system were assembled according to previously published methods [25]. Briefly, cell-free reactions contained 1.2 mM ATP; 0.85 mM each of GMP, UMP, and CMP; 30 mM phosphoenolpyruvate; 130 mM potassium glutamate; 10 mM ammonium glutamate; 12 mM magnesium glutamate; 1.5 mM spermidine; 1 mM putrescine; 34 µg/mL of folinic acid; 171 µg/mL of *E. coli* tRNA mixture; 2 mM each of 20 unlabeled amino acids; 0.33 mM NAD; 0.27 mM Coenzyme A (CoA); 4 mM potassium oxalate; 57 mM HEPES-KOH buffer (pH 7.5); 0.24% volume of the *E. coli* extract; and variable amounts of DNA switch template[26]. Reactions were carried out on a thermocycler using PCR tubes (Fisher Scientific) in volumes of 5 µL when used in the pna assay and 10 µL for the on-card assay. The source of the extract was BL21 DE3 Star prepared according to previously published protocols [25,27]. When run-off reactions were performed, 500 µL of extract was incubated in a thermomixer (Eppendorf) for 1 h at 37 °C and under shaking at 300 rpm [28]. The extract was then subjected to a 12,000 g centrifugation at 4 °C for 10 min. The supernatant was collected and stored at -80 °C. Reactions were carried out on a thermomixer (Eppendorf) using PCR tubes (Fisher Scientific) with a toehold switch template concentration of 17.5 nM. The concentration of trigger sequence was 2 µM unless otherwise stated and ddI H_2O for negative controls. 1 µL of RNAse inhibitor (Murine, New England Biolabs) were added to all reactions prior to addition of template. Cell-free reactions were also performed using the In Vitro Protein Synthesis PURExpress Kit (New England Biolabs) according the manufacturer's protocol, briefly 10 µL of

solution A, 7.5 µL of solution B, 1 µL of RNAse inhibitor, and template and trigger sequences were added to a tube. ddI H_2O was added to give the final reaction volume of 25 µL.

CFE of SBT(n) activity was assayed using 5 µL CFE reaction, 94 µL of ddI H_2O, and 1 µL of N-succinyl-Ala-Ala-Pro-Phep-nitroanilide (pna, Sigma Aldrich) and measuring absorbance at 410 nm after 30 minutes. The activity was also tested on the GSR sensor using 4x10 µL CFE reactions each diluted in 20 µL of PBS buffer (pH 7.4) and placed on the four ports of the sensor and analyzed according to previously described methods monitoring for frequency shifts.

Viral Sample RNA Extraction

All viral samples were obtained from BEI Resources/ATCC unless otherwise noted. Two heat-inactivated SARS-CoV-2 samples were used for detection: heat-inactivated culture fluid containing Hong Kong/VM20001061/2020 (HK, ZeptoMetrix) and cell lysate containing 2019-nCoV/USA-WA1/2020 (WA). Other viral samples used to screen for specificity included irradiated SARS-CoV-1 in PBS, genomic RNA from coronavirus OC43, genomic RNA from coronavirus NL63, and genomic RNA from coronavirus 229E. Viral RNA was purified according to previous methods using a QIAamp Viral RNA Mini Kit (Qiagen) according to the manufacturer's protocols[29]. Briefly, 140 µL of viral sample was combined in a 1.5 mL tube with 560 µL of AVL buffer with 5 µg of carrier RNA. This mixture was briefly vortexed and allowed to incubate at room temperature for 10 min. Following incubation, 560 µL of 100% ethanol was added before another brief vortex step. The solution was transferred to a spin column and centrifuged at 6,000 g for 1 min. 500 µL of AW1 buffer was added and the solution was centrifuged at 6,000 g for 1 min. In the final wash step, 500 µL of AW2 buffer was added and the solution was centrifuged at 20,000 g for 3 min. The viral RNA was then eluted in two volumes of 40 µL AVE buffer (for a total of 80 µL) with a 6,000 g centrifugation step for 1 min for both volumes of AVE.

Results and Discussion

Simulation of Resonant Sensor and Validation

A simulation of the sensor was made in a finite element method (FEM) software, Ansys HFSS, to simulate frequency shifts based upon a completely wet versus dry cards. The completely wet card had a frequency shift of 64.74 MHz demonstrating significant potential for a clear binary response sensor (Fig. 2a,b).

To validate these results obtained *in silico*, tests were done to measure relative changes in reactance of the GSR. Six GSR cards were prepared without gel switches in the ports to allow for free flow of fluid down to the resonator. Half remained dry and half were loaded with 30 µL

of PBS buffer into each port and then sealed in an envelope. Determination of optimal sample liquid volume to overcome evaporation loss and consistent degradation of gelatin films is described in Supplement 4. An impedance analyzer outfitted with a dielectric test meter was used to test the samples as depicted in Fig. 2c. Reactance was measured at 35 MHz to determine the effect that the fluid had on the GSR card. Wet cards had an average reactance of -0.8589±0.015 Ω and dry cards had an average reactance of -1.0022±0.086 Ω with a p-value of 0.0013 (Fig. 2d), indicating that the change in reactance to the GSR card was due to the fluid wetting the card. Note these reactance measurements included reactance from the test fixture itself, but changes were solely attributed to the card being wet or dry.

The GSR card contains four gelatin ports covering the edges of four wax-printed channels in the top layer (Fig. 2e). Wax-printed channels are used to guide fluid from the degraded gelatin to laser-cut channels towards the resonant coil layer (Fig. 2f). We determined that the fluid transfer to the resonant coil would cause a sufficient shift in the resonant frequency signal to provide a clear sensor response.

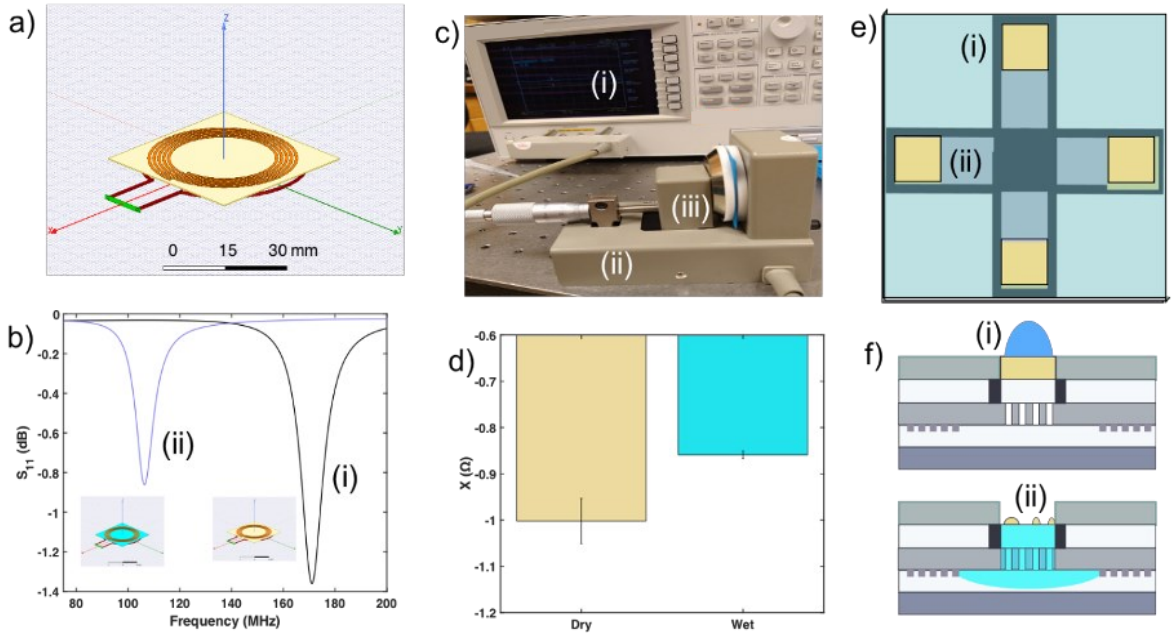

Figure 2. a) Ansys HFSS simulation setup for GSR card resonator with reader coil below the card (partially shown). b) Results of the HFSS resonant sensor simulation with (i) dry and (ii) wet signal notches c) Dielectric experiment setup with (i) impedance network analyzer, (ii) dielectric test fixture, (iii) GSR card in test fixture d) Relative reactance of the dry versus wet GSR card in dielectric test fixture e) Top view of the GSR sensor card with (i) gelatin switch and (ii) wax-printed channels. f) Side view of GSR sensor card (i) before sample degradation of gelatin switch and (ii) after sample degradation of gelatin switch.

GSR Card Fabrication

Resonant sensors are fabricated as a planar spiral coil which has an inherent inductance from the wound coil and parasitic capacitance arising from fringing fields between the arms of the

coil (Fig. 3a)[30]. This inductance (L) and capacitance (C) make the resonant sensor an effective LC tank with a self-resonant frequency being a function of the LC parameters. The inductance can be computed directly from the geometry of the spiral[31]. Parasitic capacitance is a function of the relative permittivity of the substrate in the vicinity of the resonant coil. The resonant sensor is wirelessly interrogated through non-metallic materials which allows for contact-free analysis of the sensor (Fig. 3b). Positional sensitivity between the GSR card and reader antenna were mitigated by using a linear translation stage and taking multiple scans at different positions minimizes noise of positional alignment sensitivity by taking the maximum frequency response as a reference point[32]. This allowed for the resonant frequency to be compared between scans before and after tests.

Based upon previous work,[33] it was hypothesized that degradation of a thin gelatin film would lead to a resonant frequency shift as degraded gelatin traveled from the edges of the wax printed channels down to the resonant sensor paper in the card. This was validated on card by monitoring the resonant frequency via the S_{11} scattering parameter change before and immediately after degradation of the gelatin film via protease digestion. It is important to note that the shift in resonant frequency is due to flow of fluid to the resonant sensor layer and not due to the degradation of the gelatin alone. The sensor frequency shift was monitored over time to determine the stability of the response. Since the frequency shift was a result of moisture imbibing into the resonator layer of the GSR card, it will eventually shift back to the frequency prior to degradation due to evaporation after 2 or more days, see Supplement 5.

The GSR card was coupled to cell-free expression governed by toehold switches, mRNAs with secondary structures that inhibit translation of the reporter enzyme. Upon binding of a complementary RNA strand, this structure relaxes, and translation can occur in a cell-free reaction without inhibition. For this study, a protease reporter protein was chosen to degrade the gel switch and “switch on” the GSR in the presence of a viral target. The reactions were placed in the sample ports of the GSR card and allowed time to incubate. Digestion of the gelatin would then indicate the presence of SARS-CoV-2 (Fig. 3c).

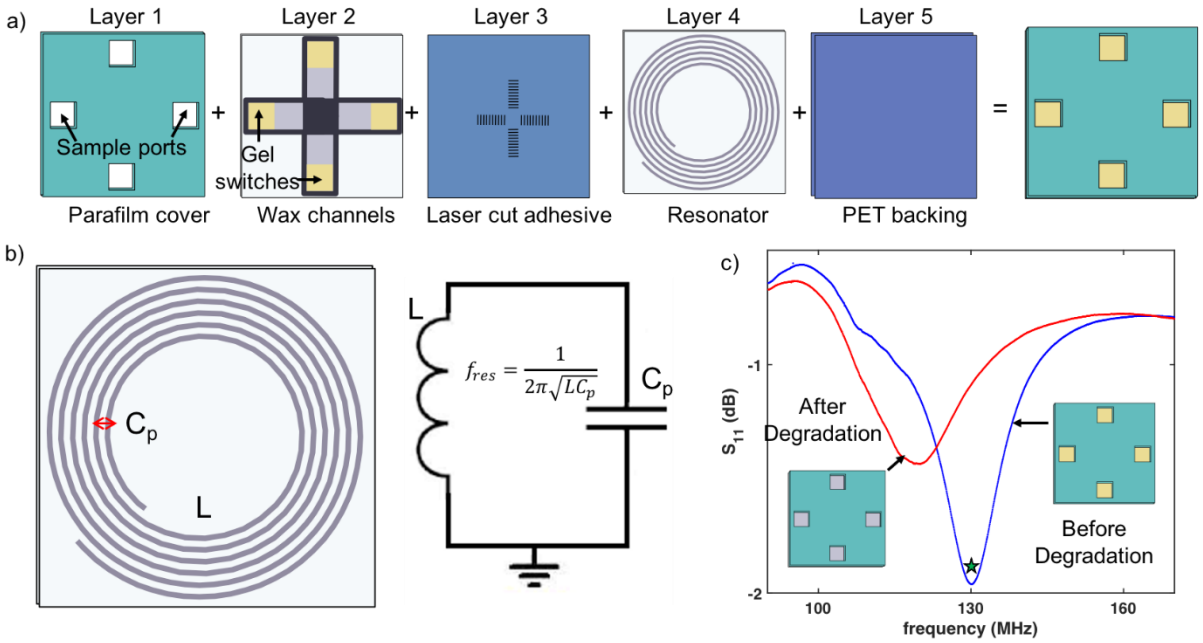

Figure 3. a) Layers of the Gel switch resonator (GSR) card device. B) Equivalent circuit diagram of the resonant layer of GSR card with relationship to f_{res}. C) Proof of concept of GSR showing frequency shift with degradation of gelatin, star indicates the resonant frequency f_{res}..

Effect of Gelatin Switch Degradation on Resonant Frequency

The sensitivity of the gelatin degradation was investigated by scanning before and after degradation of the gelatin switch by a protease (Fig. 4a). Increased sensitivity was observed in simulation by increasing the number of gelatin switches regions on the GSR card and this was supported by empirical studies, where we found that four regions provided a robust frequency shift over background, see Supplement 6 and supplementary_materials_2.aedt. From these results four ports were chosen to improve sensor sensitivity while limiting the amount of reagents for CFE reactions needed. A sample Bode plot is shown in Fig. 4b,c for a card with PBS buffer sample and diluted protease sample respectively. Note the unchanging resonant frequency of the GSR card that received the PBS buffer control sample compared with the protease sample. Three cards for PBS and protease samples were averaged and their relative change in resonant frequency are shown in bar plot in Fig. 4e. Note the 1.25 MHz frequency shift was much less than the 64 MHz predicted in the simulation. This discrepancy is likely due to the simulation analyzed with a completely wetted paper on the resonator versus this test which used a total volume of 120 µL on the paper. A larger frequency shift in the actual system is possible, if more liquid volume from sample was used; however, this would come at an increased cost in reagents per sensor device.

It is important to note here that PBS and bacterial protease were used as the negative and positive controls for the GSR sensor in this study. For a robust, mail-in platform there would need to be a second positive control to ensure proper operation by an end-user, similar to the second line on a lateral flow assay (e.g., rapid antigen tests). This would require the use of a

second reaction zone on the GSR card with toehold switches that were triggered by housekeeping genes found in saliva.

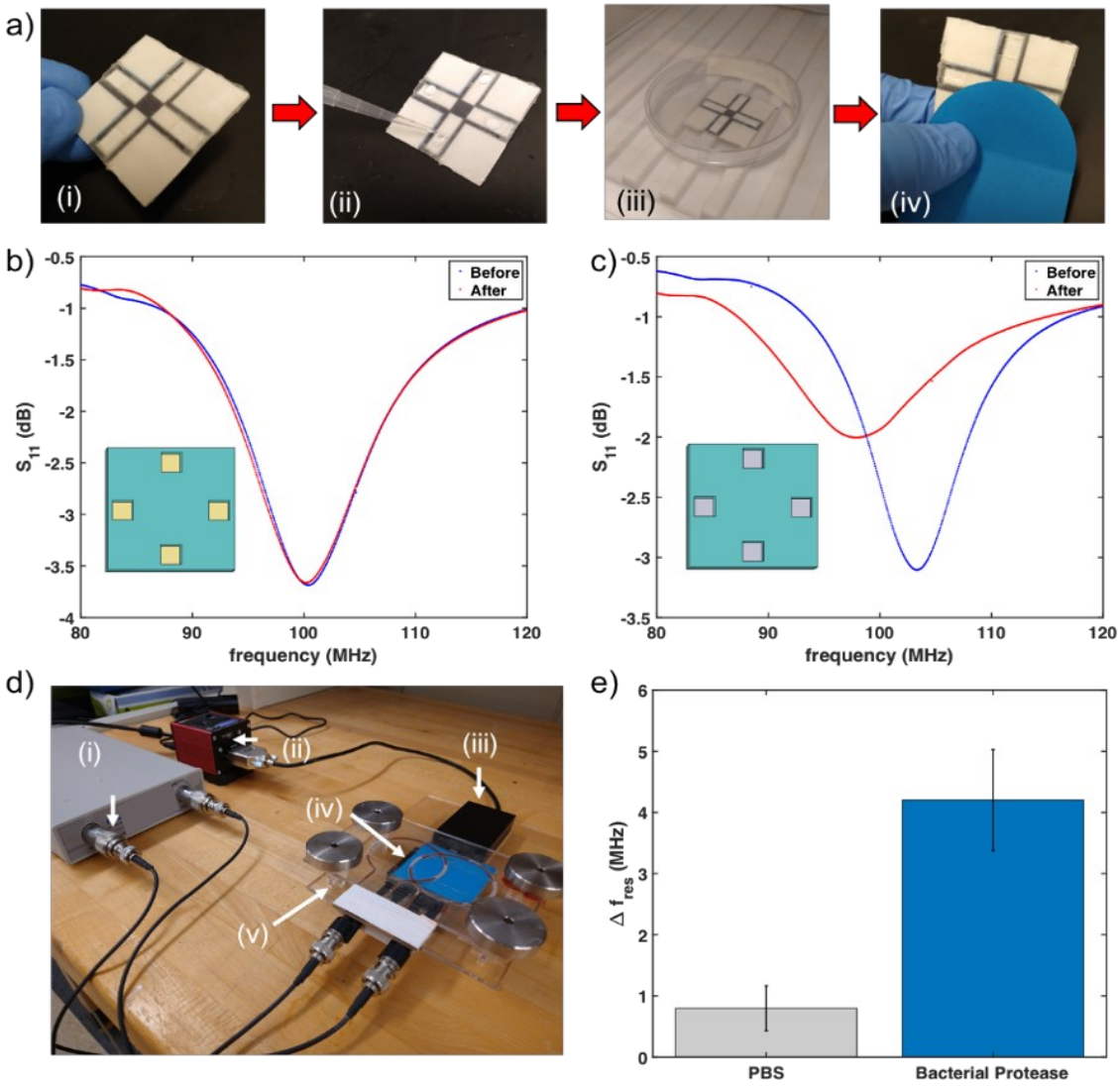

Figure 4. a) GSR test protocol (i) GSR sensor card, (ii) sample application on ports, (iii) incubation at 30 °C, (iv) sealing test in envelope after incubation b) Bode plot of resonator before and after being tested with PBS buffer for control c) Bode plot of resonator before and after being tested with bacterial protease d) Reader setup (i) VNA, (ii) linear stage controller, (iii) linear stage, (iv) sensor in envelope, (v) custom coil reader antenna. e) Bar chart of delta frequency comparing pbs buffer and subtilisin shift, error bars are standard error, n = 3.

Toehold Switch Design and Validation

Toehold switches were used for the biological recognition/transduction mechanism[22] (Fig. 5a). The term toehold refers to the single-stranded region at the 5' end of the toehold switch that is used for initial binding to the trigger RNA. The downstream stem-loop structure suppresses translation by sequestering both the ribosome binding site (RBS) and the start codon. The stem-loop structure is disrupted when the toehold switch meets its complementary trigger sequence present in the viral RNA. For this project, toehold switches were designed with specificity to the

SARS-CoV-2 N gene. Linear DNA constructs harboring the toehold sequences were initially screened in PURExpress cell-free expression system using *LacZ* as a reporter gene, which catalyzes cleavage of a yellow substrate termed Chlorophenol red-β-D-galactopyranoside and produces a purple product. This initial screening identified which switches provided the strongest response while maintaining a low background signal. Of the 11 switches tested, the N gene-S1 switch is able to quickly activate gene expression upon trigger activation and provided an ON/OFF ratio above 40; therefore, the N-gene toehold switch and S1 trigger sequence were selected for further testing (Fig. 5b).

Since the resonators work by detecting the degradation of gelatin, the next step was to identify a protease that could both efficiently degrade the gelatin substrate and be expressed using CFE. Using an azocoll assay to screen potential protease reporter candidates, we used in-house cell-free components to express a gelatinase (gelE), tobacco etch virus protease (TEV), 3 chymotrypsin-like protease (3CL), and subtilisin BPN' (SBT(n)). Bacterial protease concentrate purchased from a Carolina Biologic was used as a positive control. The expressed SBT(n) was the only cell-free candidate to exhibit activity on the azocoll substrate and was thus selected as the reporter protein, see Supplementary 7. Expression of a protease is inherently difficult as it will begin to degrade the CFE machinery necessary for protein synthesis. As a result, a protease might not be the best canddiate, but was chosen as we had demonstrated expression of proteolytic enzymes in cell-free previously[34]. For future iterations of the platform, it would be beneficial to investigate the expression of other hydrolytic enzymes and their respective hydrogel substrates for use with a GSR sensor (e.g. agarase and agar).

Although the platform described here focuses on the detection of SARS-CoV-2, the approach can be adapted for detection of other pathogens in general[24]. The following steps can be taken to adapt the toehold switch-GSR platform to target other viruses. First, identify the RNA/DNA sequences specific to the targets of interests from published literature or sequence databases. Second, use these sequences to generate target-specific toehold switches using NUPACK[21,35]-based algorithms[36]. Third, assemble the toehold switches with fluorogenic or chromogenic reporters for rapid empirical validation using cell-free systems. Based on performance, functional toehold switches can then be selected and assembled with the appropriate hydrolase reporter (e.g. subtilisin) sequences to interface with gel switch resonators. The toehold sensor development stage only takes approximately five days and therefore allows a timely response to new pathogens once their sequences are known. In some cases, such as differentiating SARS-CoV-2 variants, where higher sequence specificity is required, ultra-specific riboregulators termed single-nucleotide-specific programmable riboregulators[37] (SNIPRs) have been developed. SNIPRs allow sequences that are closely related and/or highly similar to be distinguished. The SNIPR design algorithm is available at https://github.com/Albert09111/SNIPR. The remaining GSR platform (gel patterned papers) would not need to be adapted and could be stock-piled for rapid pandemic response. The new toehold sequences would be formulated and dried on the cards, and they would be ready for shipment.

The extent of toehold switch activation is correlated with the amount of trigger RNA present in the reaction, and this must be amplified from low viral copy counts to provide enough sensitivity. Amplification of trigger RNA was done using RT-RPA as it is an isothermal amplification method that can theoretically be performed at room temperature, or for better results at body temperature[38]. It is important to ensure that the RPA reaction produces enough cDNA at a fast enough rate to support downstream reverse transcription of trigger RNA. Multiple combinations of forward and reverse primers for toehold switches encoding N-gene with S1 trigger sequence were designed *in silico* and screened for their efficiency. RT-RPA was conducted for 10 minutes at 30 °C before being heat inactivated and run on a gel. The primer combinations resulting in the brightest bands were determined to be the most efficient because of their ability to produce amplified cDNA quickly (data not shown). These primers were used in all subsequent experiments. This unit operation would need to be simplified for a practical mail-in platform as, in the current state, it requires combination of several reagents in a tube off the card and subsequent incubation at a set temperature. For optimal work-flow as a simple mail-in platform, the virus lysis and RNA amplification should be incorporated into the paper platform, where only liquid sample is applied and incubated at room temperature[18].

The switches containing SBT(n) were expressed in PURExpress for initial proof of concept studies. These studies used toehold switches encoded as linear expression templates and expressed using the PURExpress kit. Activity was then measured using a N-SUCCINYL-ALA-ALA-PRO-PHE-P-NITROANILIDE (pna) assay. Samples from the reactions were assayed for 30 min to ensure sufficient metabolism of pna substrate by SBT(n). Reactions were either dosed with complementary trigger RNA encoding the target SARS-CoV-2 sequence or water. In the presence of the trigger RNA, a clear non-linear increase in signal can be observed, whereas the reactions with water show no increase. Toehold switch with N-gene and S1 trigger sequence were then put into plasmids for transformation and propagation. The limit of detection (LOD) for this switch was found to be 100 copies/µL, see Supplement 8.

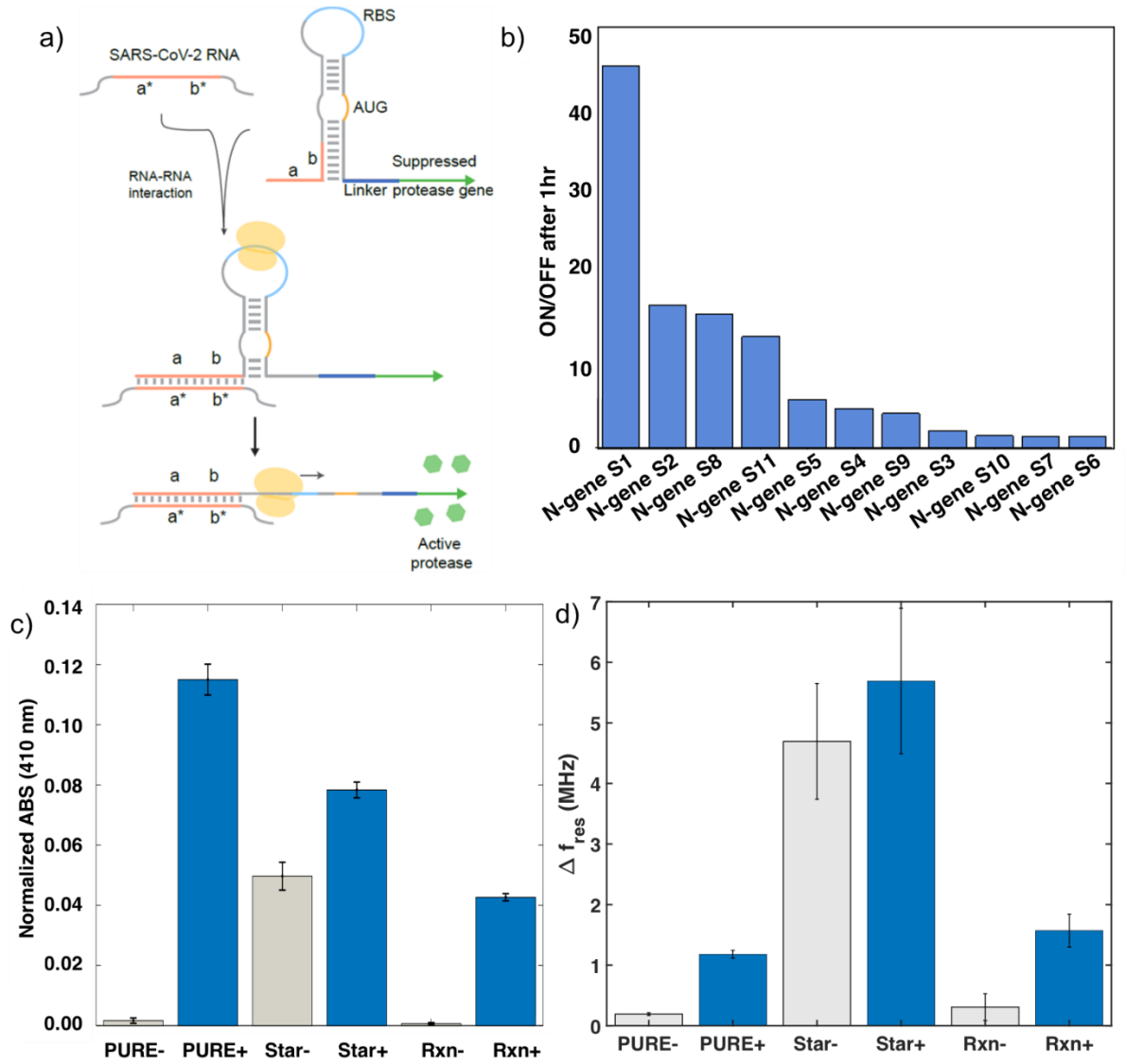

Figure 5. a) Schematic diagram of toehold switch mechanism. b) Toehold switch initial screening of designed toehold switch and trigger sequences. c) pna assay of toehold switch in different cell-free expression systems, PURE is PURExpress (NEB), Star is BL21 DE3 lysate without run-off reaction and Rxn is BL21 DE3* lysate with run-off, note + means with trigger RNA and – means without trigger RNA. d) GSR test results in different cell-free expression systems, error bars denote standard error, n = 3.*

CFE Reaction on GSR Card with Viral Samples and Mail-in Test

To optimize the CFE conditions for toehold switch activity, a two-factor designed experiment (DOE) was performed to optimize toehold switch plasmid concentration and CFE reaction time, see Supplement 9. Although the results of the DOE indicate a concentration outside of the design space could be even more productive, a toehold switch concentration of 17.5 nM and cell-free reaction time of 5 hours were chosen to minimize plasmid cost and also set a reaction time that would be able to be performed in an 8 hour workday. The switch concentration of

17.5 nM is a relatively low concentration compared to literature values, but this optimum is likely protein dependent [39]. These reaction conditions were used in all experiments hereafter.

In order to develop a more cost-effective system to the more expensive recombinant CFE reagents (PURExpress), in-house CFE components were prepared using extract from BL21 DE3 Star and an PANOx-SP energy mix[26]. As a proof of concept, CFE reactions using PURExpress reagents, BL21 DE3 Star extract, and BL21 DE3 Star extract that had undergone a 1-h run-off reaction were tested using the pna assay. The PURExpress reactions result in a strong response with a 4.32x increase in signal when the trigger RNA was added (Fig 5c). Meanwhile in-house components (with no run-off reaction) result in having a high background and poor frequency shift discrepancy on the GSR card. However, upon performing a 1-h run-off reaction on the BL21 DE3 Star extract, an increase in activity of 2.08x is achieved with a good signal-to-noise ratio on the GSR card (Fig. 5d).

This finding seems counterintuitive since literature has shown that BL21 DE3 Star extract does not show an increase in protein synthesis after a run-off reaction when the gene of interest is behind a T7 promoter [40]. Nevertheless, BL21 DE3 Star extract has been shown to work with toehold switches in the past when subjected to a 1-hour run-off reaction [28]. It is important to note that raw signal from extract that has not undergone a run-off reaction is much higher than that of extract that has undergone a run-off reaction. This is due to the turbid nature of this extract. Performing a run-off reaction drastically reduces the turbidity of the extract thus reducing the artificially inflated signal (Fig 5c). The successful PURExpress and BL21 DE3 Star extract that had undergone a run-off reaction were then tested on GSR cards. The in-house CFE performed similar to the PURExpress system on card with a frequency shift between conditions with 2.5 µM trigger sequence and without the trigger of 1.23 MHz compared to 1.36 MHz for the PURE system, Fig. 5d.

The GSR card was then tested for potential as a mail-in platform. The sensor was initially placed in an envelope in Ames, IA and scanned before being shipped overnight to collaborators in Toronto, ON. There, a cell-free reaction with N-gene plasmid with synthetic S1 trigger sequences was placed on top of the GSR card and incubated at 30 °C for 5 hours to allow for proper degradation of gelatin switch. After the incubation period was complete, the sensors were sealed in an envelope and shipped to the automated scanner in Ames, IA for contact-free analysis inside the sealed envelope, Fig. 6a. These results demonstrate the potential to use the GSR card as a mail-in testing platform for convenient drop-off and scanning of confidential samples at a centralized work, school, or medical facility. However, in order for this platform to be a viable as a mail-in platform, the other off chip steps will have to be mitigated to make them simpler for the end-user.

Finally, specificity was assessed by testing viral samples from different coronaviruses. Two positive samples were from separate SARS-CoV-2 isolates: 2019-nCoV/USA-WA1/2020 from cell lysate and Hong Kong/VM20001061/2020 from cell culture fluid. Challenge viruses included SARS-CoV-1, three seasonal strains 229E, OC43, and NL63. All samples were purified using an RNA extraction kit and subject to RT-RPA using the same primers for the N C7 switch followed

by *in vitro* transcription. These transcripts were then added to in-house CFE reactions as triggers. After incubation 30 °C for 5 hours , the CFE reactions were transferred to the GSR cards. Following a 5 hour incubation on the GSR cards, toehold switches were able to clearly discriminate the SARS-CoV-2 virus strains (HK and WA) over SARS-CoV-1 and the other common, seasonal coronaviruses (Fig. 6c).

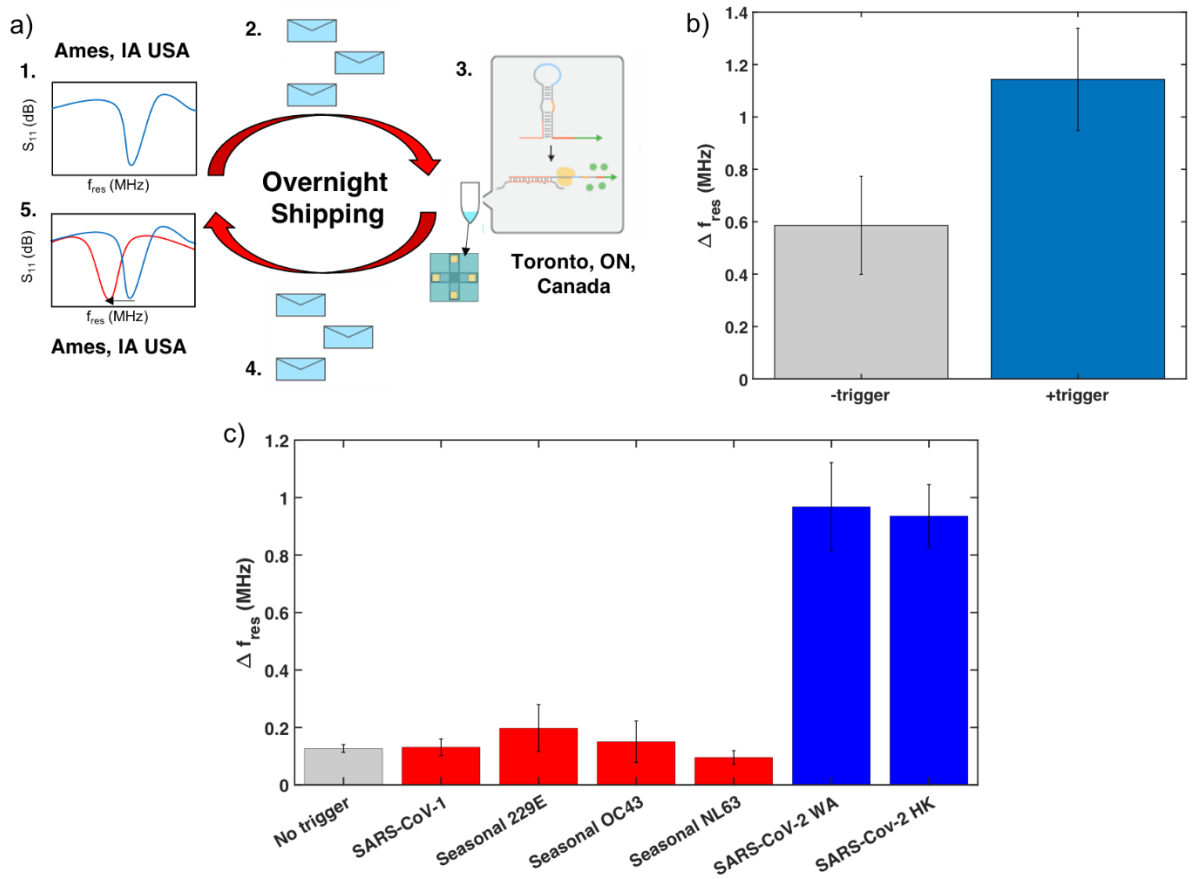

Figure 6. a) Mail-in test using overnight shipping between Ames, IA and Toronto, ON. b) Frequency shift results from mail-in test. c) Specificity of GSR card sensor to different coronavirus SARS (SARS-CoV-1), seasonal (229E, OC43, NL63), and SARS-CoV-2 (WA, HK).

Conclusion

A riboregulator, toehold switch, with a protease reporter enzyme, SBT(N), was designed and optimized for degradation of the gelatin switch in the GSR card. The toehold switch utilized the N gene from SARS-CoV-2 genome as the recognition site which was found to be both specific over other coronaviruses and sensitive, with a LOD of 100 copies/µL. The use of a modular toehold switch allows for rapid adaption of this platform to detect other pathogens of interest. Mailing the sealed GSR card after exposure to trigger RNA and reading on a centralized scanner was successfully demonstrated, however a clear signal does not persist beyond three days. To improve signal stability and performance future work will include incorporating hygroscopic

materials and impermeable membranes to reduce water vapor loss. This platform has the promise to provide an efficient pandemic screening solution across remote locations that are not suitable for mass sample collection sites. Moreover, the platform should be readily adapted to future pandemic threats by rapidly swapping out the toe-hold switch sequence for other target RNA sequences. The ability of cell-free systems to detect a variety of molecular analytes and the mail-in capabilities of the platform suggest that it could be used more broadly for other environmental monitoring purposes. Such sensors could be used to provide spatially defined early warning of outbreaks in wastewater, monitoring of mosquito populations for malaria and viral infections, and water quality testing with results compiled and assessed at a centralized location.

A unique, contact-free sensing platform was developed for detection of viral RNA by combining planar resonant sensors and toehold switch technology. The sensor provides a clear, binary, digital readout that can be interrogated through a sealed envelope. Sealed samples have the advantage of enabling test analysis without the need of PPE, enabling limited supplies to be used for more critical purposes. This sensor also has the potential to be used as a mail-in platform, thereby allowing for convenient aggregation of public health data from dense urban and rural locations. For further development of the platform, as a practical mail-in test, the unit operations for viral sampling, RNA extraction, and isothermal amplification will have to be further developed for ease of use; quality of results will likely be affected by end users having to currently perform multiple off-GSR card steps to prepare the sample. Another crucial design addition isinclusion of a clear positive control with a toehold switch triggered by mRNA regularly found in samples. Further work could be done on the reader system to make it low-cost enough for at home adoption, thereby allowing for analysis of the paper cards to be done at home and still allowing for cloud aggregation of the public health data.

Acknowledgements

A.R.C, J.L.P, N.F.R. were supported by an NSF RAPID Grant Award Number (FAIN): 1827578 and by an NSF PFI IIP Grant Award Number (FAIN): 2029352.

K.W. and A.A.G. were supported by an NSF RAPID Grant Award Number (FAIN): 1827578

P.S.M. was supported by an NSERC Alexander Graham Bell Canada Graduate Scholarship (CGS-D).

K.P. was support by funds from the Canada's International Development Research Centre (grant 109434-001) through the Canadian 2019 Novel Coronavirus (COVID-19) Rapid Research Funding Opportunity and the University of Toronto COVID-19 Action Initiative 2020.

Supporting information

The Supporting Information: is available free of charge.

Resonant sensor noise reduction method, Matlab scripts for GSR card data analysis, target sequence of toehold switch, gel height thickness and degradation properties, frequency shift stability, HFSS simulation multiple gelatin switches, azocoll assay for protease screening, limit of detection, and optimization of toehold switch concentration and reaction time.

References

(1) Sturmberg, J. P.; Martin, C. M. COVID-19 – How a Pandemic Reveals That Everything Is Connected to Everything Else. *J. Eval. Clin. Pract.* **2020**, *26* (5), 1361–1367. https://doi.org/10.1111/jep.13419.

(2) Bai, Y.; Yao, L.; Wei, T.; Tian, F.; Jin, D. Y.; Chen, L.; Wang, M. Presumed Asymptomatic Carrier Transmission of COVID-19. *JAMA - Journal of the American Medical Association*. American Medical Association April 2020, pp 1406–1407. https://doi.org/10.1001/jama.2020.2565.

(3) Rothe, C.; Schunk, M.; Sothmann, P.; Bretzel, G.; Froeschl, G.; Wallrauch, C.; Zimmer, T.; Thiel, V.; Janke, C.; Guggemos, W.; Seilmaier, M.; Drosten, C.; Vollmar, P.; Zwirglmaier, K.; Zange, S.; Wölfel, R.; Hoelscher, M. Transmission of 2019-NCoV Infection from an Asymptomatic Contact in Germany. *N. Engl. J. Med.* **2020**, *382* (10), 970–971. https://doi.org/10.1056/nejmc2001468.

(4) Chu, D. K. W.; Pan, Y.; Cheng, S. M. S.; Hui, K. P. Y.; Krishnan, P.; Liu, Y.; Ng, D. Y. M.; Wan, C. K. C.; Yang, P.; Wang, Q.; Peiris, M.; Poon, L. L. M. Molecular Diagnosis of a Novel Coronavirus (2019-NCoV) Causing an Outbreak of Pneumonia. *Clin. Chem.* **2020**, *66* (4), 549–555. https://doi.org/10.1093/clinchem/hvaa029.

(5) Wang, W.; Xu, Y.; Gao, R.; Lu, R.; Han, K.; Wu, G.; Tan, W. Detection of SARS-CoV-2 in Different Types of Clinical Specimens. *JAMA - Journal of the American Medical Association*. American Medical Association 2020. https://doi.org/10.1001/jama.2020.3786.

(6) Abbasi, K. Covid-19: Screening without Scrutiny, Spending Taxpayers' Billions. *The BMJ*. BMJ Publishing Group November 2020. https://doi.org/10.1136/bmj.m4487.

(7) Kucirka, L. M.; Lauer, S. A.; Laeyendecker, O.; Boon, D.; Lessler, J. Variation in False-Negative Rate of Reverse Transcriptase Polymerase Chain Reaction-Based SARS-CoV-2 Tests by Time Since Exposure. *Annals of internal medicine*. NLM (Medline) August 2020, pp 262–267. https://doi.org/10.7326/M20-1495.

(8) Woloshin, S.; Patel, N.; Kesselheim, A. S. False Negative Tests for SARS-CoV-2 Infection — Challenges and Implications. *N. Engl. J. Med.* **2020**, *383* (6), e38. https://doi.org/10.1056/nejmp2015897.

(9) Kanji, J. N.; Zelyas, N.; MacDonald, C.; Pabbaraju, K.; Khan, M. N.; Prasad, A.; Hu, J.; Diggle, M.; Berenger, B. M.; Tipples, G. False Negative Rate of COVID-19 PCR Testing: A Discordant Testing Analysis. *Virol. J.* **2021**, *18* (1), 1–6. https://doi.org/10.1186/s12985-021-01489-0.

(10) Surkova, E.; Nikolayevskyy, V.; Drobniewski, F. False-Positive COVID-19 Results: Hidden Problems and Costs. *Lancet Respir. Med.* **2020**, *8* (12), 1167–1168. https://doi.org/10.1016/S2213-2600(20)30453-7.

(11) Lazarevic, I.; Pravica, V.; Miljanovic, D.; Cupic, M. Immune Evasion of SARS-CoV-2 Emerging Variants: What Have We Learnt So Far? *Viruses* **2021**, *13* (7), 1192. https://doi.org/10.3390/v13071192.

(12) Zhang, W.; Davis, B. D.; Chen, S. S.; Sincuir Martinez, J. M.; Plummer, J. T.; Vail, E. Emergence of a Novel SARS-CoV-2 Variant in Southern California. *JAMA - J. Am. Med. Assoc.* **2021**, *325* (13), 1324–1326. https://doi.org/10.1001/jama.2021.1612.

(13) Fujino, T.; Nomoto, H.; Kutsuna, S.; Ujiie, M.; Suzuki, T.; Sato, R.; Fujimoto, T.; Kuroda, M.; Wakita, T.; Ohmagari, N. Novel SARS-CoV-2 Variant in Travelers from Brazil to Japan. *Emerg. Infect. Dis.* **2021**, *27* (4), 1243–1245. https://doi.org/10.3201/eid2704.210138.

(14) Challen, R.; Brooks-Pollock, E.; Read, J. M.; Dyson, L.; Tsaneva-Atanasova, K.; Danon, L. Risk of Mortality in Patients Infected with SARS-CoV-2 Variant of Concern 202012/1: Matched Cohort Study. *BMJ* **2021**, *372*, 1–10. https://doi.org/10.1136/bmj.n579.

(15) Tegally, H.; Wilkinson, E.; Giovanetti, M.; Iranzadeh, A.; Fonseca, V.; Giandhari, J.; Doolabh, D.; Pillay, S.; San, E. J.; Msomi, N.; Mlisana, K.; von Gottberg, A.; Walaza, S.; Allam, M.; Ismail, A.; Mohale, T.; Glass, A. J.; Engelbrecht, S.; Van Zyl, G.; Preiser, W.; Petruccione, F.; Sigal, A.; Hardie, D.; Marais, G.; Hsiao, N. yuan; Korsman, S.; Davies, M. A.; Tyers, L.; Mudau, I.; York, D.; Maslo, C.; Goedhals, D.; Abrahams, S.; Laguda-Akingba, O.; Alisoltani-Dehkordi, A.; Godzik, A.; Wibmer, C. K.; Sewell, B. T.; Lourenço, J.; Alcantara, L. C. J.; Kosakovsky Pond, S. L.; Weaver, S.; Martin, D.; Lessells, R. J.; Bhiman, J. N.; Williamson, C.; de Oliveira, T. Detection of a SARS-CoV-2 Variant of Concern in South Africa. *Nature* **2021**, *592* (7854), 438–443. https://doi.org/10.1038/s41586-021-03402-9.

(16) Karim, S. S. A.; Karim, Q. A. Omicron SARS-Cov-2 Variant: A New Chapter in the COVID-19 Pandemic. *Lancet* **2021**, *398* (10317), 2126–2128.

(17) Wang, Y.; Zhang, Y.; Chen, J.; Wang, M.; Zhang, T.; Luo, W.; Li, Y.; Wu, Y.; Zeng, B.; Zhang, K.; Deng, R.; Li, W. Detection of SARS-CoV-2 and Its Mutated Variants via CRISPR-Cas13-Based Transcription Amplification. *Anal. Chem.* **2021**, *93* (7), 3393–3402. https://doi.org/10.1021/acs.analchem.0c04303.

(18) Yu, Y.; Su, G.; Zhang, W. S.; Pan, J.; Li, F.; Zhu, M.; Xu, M.; Zhu, H. Reverse Transcription Recombinase Polymerase Amplification Coupled with CRISPR-Cas12a for Facile and Highly Sensitive Colorimetric SARS-CoV-2 Detection. *Anal. Chem.* **2021**, *93* (8), 4126–4133. https://doi.org/10.1021/acs.analchem.1c00013.

(19) Moon, J.; Kwon, H. J.; Yong, D.; Lee, I. C.; Kim, H.; Kang, H.; Lim, E. K.; Lee, K. S.; Jung, J.; Park, H. G.; Kang, T. Colorimetric Detection of SARS-CoV-2 and Drug-Resistant PH1N1 Using CRISPR/DCas9. *ACS Sensors* **2020**, *5* (12), 4017–4026. https://doi.org/10.1021/acssensors.0c01929.

(20) Charkhabi, S.; Chan, Y. J.; Roy, S.; Islam, M. M.; Duffield, B. B.; Jackson, K. J.; Bu, L.; Kim, S. H.; Hillier, A. C.; Neihart, N. M.; Reuel, N. F. Effects of Fabrication Materials and Methods on Flexible Resonant Sensor Signal Quality. *Extrem. Mech. Lett.* **2020**, *41*, 101027. https://doi.org/10.1016/j.eml.2020.101027.

(21) Zadeh, J. N.; Wolfe, B. R.; Pierce, N. A. Nucleic Acid Sequence Design via Efficient Ensemble Defect Optimization. *J. Comput. Chem.* **2011**, *32* (3), 439–452. https://doi.org/10.1002/JCC.21633.

(22) Green, A. A.; Silver, P. A.; Collins, J. J.; Yin, P. Toehold Switches: De-Novo-Designed Regulators of Gene Expression. *Cell* **2014**, *159* (4), 925–939. https://doi.org/10.1016/j.cell.2014.10.002.

(23) Ma, D.; Shen, L.; Wu, K.; Diehnelt, C. W.; Green, A. A. Low-Cost Detection of Norovirus Using Paper-Based Cell-Free Systems and Synbody-Based Viral Enrichment. *Synth. Biol.* **2018**, *3* (1), 1–11. https://doi.org/10.1093/synbio/ysy018.

(24) Pardee, K.; Green, A. A.; Takahashi, M. K.; Braff, D.; Lambert, G.; Lee, J. W.; Ferrante, T.; Ma, D.; Donghia, N.; Fan, M.; Daringer, N. M.; Bosch, I.; Dudley, D. M.; O'Connor, D. H.;

Gehrke, L.; Collins, J. J. Rapid, Low-Cost Detection of Zika Virus Using Programmable Biomolecular Components. *Cell* **2016**, *165* (5), 1255–1266. https://doi.org/10.1016/j.cell.2016.04.059.

(25) Dopp, J. L.; Jo, Y. R.; Reuel, N. F. Methods to Reduce Variability in E. Coli-Based Cell-Free Protein Expression Experiments. *Synth. Syst. Biotechnol.* **2019**, *4* (4), 204–211. https://doi.org/10.1016/j.synbio.2019.10.003.

(26) Dopp, B. J. L.; Tamiev, D. D.; Reuel, N. F. Cell-Free Supplement Mixtures: Elucidating the History and Biochemical Utility of Additives Used to Support in Vitro Protein Synthesis in E. Coli Extract. *Biotechnol. Adv.* **2019**, *37* (1), 246–258. https://doi.org/10.1016/j.biotechadv.2018.12.006.

(27) Dopp, J. L.; Reuel, N. F. Process Optimization for Scalable E. Coli Extract Preparation for Cell-Free Protein Synthesis. *Biochem. Eng. J.* **2018**, *138*, 21–28. https://doi.org/10.1016/j.bej.2018.06.021.

(28) Takahashi, M. K.; Tan, X.; Dy, A. J.; Braff, D.; Akana, R. T.; Furuta, Y.; Donghia, N.; Ananthakrishnan, A.; Collins, J. J. A Low-Cost Paper-Based Synthetic Biology Platform for Analyzing Gut Microbiota and Host Biomarkers. *Nat. Commun.* **2018**, *9* (1), 1–12. https://doi.org/10.1038/s41467-018-05864-4.

(29) Hu, B.; Dopp, J. L.; Salituro, G. M.; Rubinstein, L. J. Real-Time PCR Assay as a Simple and Efficient Tool for Viral Stability Study. *Bioanalysis* **2021**, *13* (5), 387–394. https://doi.org/10.4155/bio-2021-0002.

(30) Huang, Q. A.; Dong, L.; Wang, L. F. LC Passive Wireless Sensors Toward a Wireless Sensing Platform: Status, Prospects, and Challenges. *Journal of Microelectromechanical Systems*. 2016. https://doi.org/10.1109/JMEMS.2016.2602298.

(31) Mohan, S. S.; Hershenson, M. D. M.; Boyd, S. P.; Lee, T. H. Simple Accurate Expressions for Planar Spiral Inductances. *IEEE J. Solid-State Circuits* **1999**. https://doi.org/10.1109/4.792620.

(32) Chan, Y. J.; Carr, A. R.; Charkhabi, S.; Furnish, M.; Beierle, A. M.; Reuel, N. F. Wireless Position Sensing and Normalization of Embedded Resonant Sensors Using a Resonator Array. *Sensors Actuators, A Phys.* **2020**.

(33) Charkhabi, S.; Beierle, A. M.; McDaniel, M. D.; Reuel, N. F. Resonant Sensors for Low-Cost, Contact-Free Measurement of Hydrolytic Enzyme Activity in Closed Systems. *ACS Sensors* **2018**, *3* (8), 1489–1498. https://doi.org/10.1021/acssensors.8b00267.

(34) Dopp, J. L.; Reuel, N. F.; Rothstein, S. M.; Mansell, T. J. Rapid Prototyping of Proteins : Mail Order Gene Fragments to Assayable Proteins within 24 Hours. **2019**, No. December 2018, 667–676. https://doi.org/10.1002/bit.26912.

(35) Zadeh, J. N.; Steenberg, C. D.; Bois, J. S.; Wolfe, B. R.; Pierce, M. B.; Khan, A. R.; Dirks, R. M.; Pierce, N. A. NUPACK: Analysis and Design of Nucleic Acid Systems. *J. Comput. Chem.* **2011**, *32* (1), 170–173. https://doi.org/10.1002/JCC.21596.

(36) Wu, K.; Yan, Z.; Green, A. A. Computational Design of RNA Toehold-Mediated Translation Activators. *Riboregulators Methods Protoc.*

(37) Hong, F.; Ma, D.; Wu, K.; Mina, L. A.; Luiten, R. C.; Liu, Y.; Yan, H.; Green, A. A. Precise and Programmable Detection of Mutations Using Ultraspecific Riboregulators. *Cell* **2020**, *180* (5), 1018-1032.e16. https://doi.org/10.1016/j.cell.2020.02.011.

(38) Piepenburg, O.; Williams, C. H.; Stemple, D. L.; Armes, N. A. DNA Detection Using

Recombination Proteins. *PLoS Biol.* **2006**, *4* (7), 1115–1121. https://doi.org/10.1371/journal.pbio.0040204.

(39) Cao, M.; Sun, Q.; Zhang, X.; Ma, Y.; Wang, J. Detection and Differentiation of Respiratory Syncytial Virus Subgroups A and B with Colorimetric Toehold Switch Sensors in a Paper-Based Cell-Free System. *Biosens. Bioelectron.* **2021**, *182* (January). https://doi.org/10.1016/j.bios.2021.113173.

(40) Kwon, Y. C.; Jewett, M. C. High-Throughput Preparation Methods of Crude Extract for Robust Cell-Free Protein Synthesis. *Sci. Rep.* **2015**, *5*, 1–8. https://doi.org/10.1038/srep08663.